ECLÉTICA QUÍMICA

Eclet. Quim. 51 | e-1546, 2026

Original Articles in Chemistry and Related Areas

https://doi.org/10.26850/1678-4618.eq.v51.2026.e1546

Synthesis, description and optical activity of silver nanoparticles electrogeneration system in various stabilizers

Hayder Khudhair **Khattar**[1+], Zainab Abdul-Zahra **Abdul-Hassan**[1], Emad Abbas Jaffar **Al-Mulla**[1,2]

Abstract

Silver nanoparticles can be synthesized via several methods, with electrogeneration being one of the most dynamic cost-effective techniques. This offers precise control for shape and size of nanoparticles, making it superior to other strategies. Stabilizers as Glycerin (GLY.), Polyvinyl alcohol (PVA), and Polyvinylpyrrolidone (PVP) were used to prevent aggregation, promote the growth and nucleation of suspended particles. In this study, multiple analytical tools, including (XRD), (FESEM), and (HRTEM), were employed to characterize synthesized Ag NPs. Prepared Ag NPs were calcined at 300 °C to remove impurities. The prepared Ag NPS in the presence of PVA were selected for the photocatalytic process, because they have a wide surface area and small particles sizes of about ~60.51 nm, after calcination at 300 °C. The photodegradation efficiency was 98.60% for the standard Ag NPs and 95.70% for the synthesized. The reactions followed pseudo-first-order kinetics, characterized by the Langmuir-Hinshelwood model. The activation energy (Ea) was 14.737 kJ mol^{-1} for the standard Ag NPs and 13.483 kJ mol^{-1} for the synthesized Ag NPs.

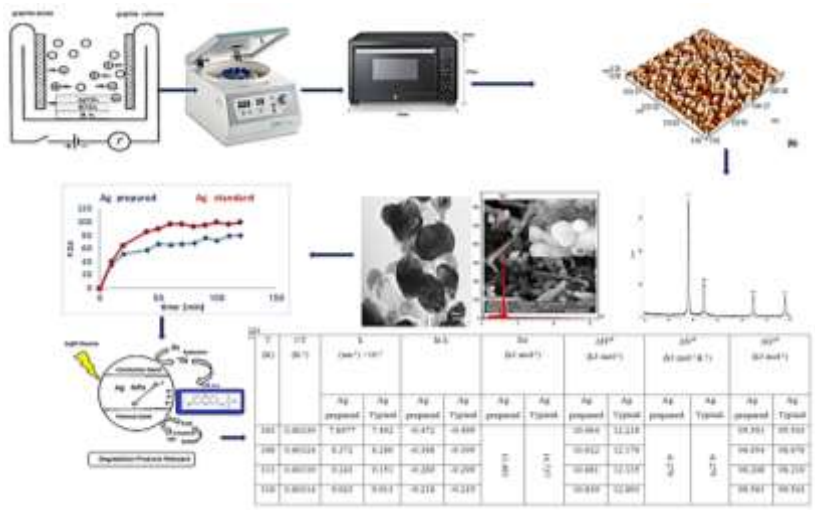

Article History

Received March 08, 2025
Accepted September 18, 2025
Published August 07, 2026

Keywords

1. electrochemical;
2. photocatalysis;
3. enthalpy;
4. activation energy.

Section Editors

Manuel Ignacio Azocar **Guzmán**

Highlights

- Electrogeneration with among the most efficient and cost-effective techniques.
- This method offers precise control over the shape and size of nanoparticles.
- A mechanism using photocatalysis using silver nanoparticles is proposed.
- The effect of pH, temperature, dye concentration, $\Delta H^{o\#}$, $\Delta S^{o\#}$ and $\Delta G^{o\#}$ were discussed.

[1]Al-Furat Al-Awsat Technical University, College of Health and Medical Techniques, An-Najaf, Iraq. [2]The Islamic University, College of Medical Technology, An-Najaf, Iraq. **+Corresponding author:** Hayder Khudhair Khattar, **Phone:** +9647829835209, **Email address:** haider.khattarckm11@atu.edu.iq

1. Introduction

Nanotechnology involves manipulating and controlling matter at the nanoscale, typically below 100 nm. Nanoparticles exhibit unique properties that differ significantly from their bulk counterparts (Roco *et al.*, 2011). Recently, nanoparticles have gained significant attention for applications in diverse fields. Silver nanoparticles are widely used as chemical catalysts (Zhang *et al.*, 2016), antibacterial agents (Shende *et al.*, 2017), sensors (Nia *et al.*, 2015), and superconductors (Xue *et al.*, 2012). They are also applied in optics due to their remarkable catalytic, electrochemical, and conductive properties (Bharadwaj *et al.*, 2021). Silver NPs exhibit properties that depend on their distribution and morphology, influencing their optical, magnetic, and electrochemical applications (Khedkar *et al.*, 2023). Various synthesis methods for Ag NPs include gamma irradiation (Naganthran *et al.*, 2022), chemical reduction (Abdellatif *et al.*, 2022), photoreduction in dye removal processes (Ghobashy *et al.*, 2021), and electrochemical techniques (Meena and Santhakumar, 2022). Among these, electrochemical synthesis is rapid, eco-friendly, and allows precise control over nanoparticles' size and morphology by adjusting current and voltage (Yin *et al.*, 2020). Silver nanoparticles have shown excellent utility in biological applications, including photocatalysis and optical sensing (Haryono *et al.*, 2008). The photocatalytic activity of Ag NPs has been extensively reported (Fairuzi *et al.*, 2018). Saeed *et al.* (2015) showed that homeopathic methylene blue dye could be degraded within 72 h at a rate of 95%. Furthermore, methylene orange dye was effectively degraded by 90% within six hours at pH=2 using a photocatalyst derived from polyacrylonitrile nanofiber-modified AgNPs. Additionally, silver nanoparticles can reduce 98.3% of methylene blue (6B) dye within four hours and methylene orange dye within one hour (Sinha *et al.*, 2016). Bhanage and Kulkarni (2014) and Jyoti and Singh (2016) demonstrated the degradation of methyl orange and methylene blue dyes using Ag NPs synthesized with sugarcane sap. Jyoti and Singh's method achieved a complete reduction of dyes in less than 21 min. Moreover, silver nanoparticles synthesized from *Zanthoxylum armatum* leaves showed rapid and efficient degradation of various dyes. The main aim of this search is to synthesize and characterize Ag-based nanoparticles using an electrochemical method and esteem their photocatalytic efficiency in degrading organic dyes under UV light. This work aims to enhance the understanding of how different stabilizers and processing conditions influence nanoparticle size and structure.

2. Materials and methods

The electrochemical synthesis of Ag NPs involves controlling size and shape by adjusting current density, voltage and electrolyte additives (**Table 1**). This setup includes two inert electrodes from a graphite anode and a cathode, each measuring 2 cm x 3 cm x 4 mm. A graphite anode is often preferred over other inert materials because it's chemically stable, a good conductor, and does not actively participate in the electrochemical reaction. It is very weakly reactive and does not undergo sacrificial degradation. The electrodes are positioned vertically facing each other with a 2 cm gap. The system is placed in an electrochemical cell containing 100 mL of deionized water (DW). During the electrogeneration process, silver nanoparticles are formed on the cathode. It was observed during the preparation process that the resulting deposit tends to gather at the bottom of the cell. The process operates at 40 °C using a 15 V DC power supply (Maximum: 30 V, 5 A, China). A voltmeter monitors the current during deposition, with a fixed time interval of five minutes (Raposo *et al.*, 2007). The electrochemical bath was composed of $AgNO_3$ (1 g/100 mL) and KNO_3 (0.03 g/100 mL) as the precipitation electrolyte, with 10 mL of other stabilizers (PVP, PVA, or Glycerin) were added to improve particle stability, mixed and then diluted to a final volume of 100 mL; concentrations refer to the final working solution. The bath pH was adjusted to ~7 using NaOH or HNO_3 as needed. A neutral pH was selected to prevent premature hydrolysis of Ag^+ ions and to maintain stability of the stabilizing agents (PVP, PVA and glycerin). A current density of 500 mA/m² was applied, based on literature values and preliminary tests, to allow controlled silver ion reduction at the cathode surface. Lower current densities resulted in incomplete reduction, while higher densities led to dendritic growth polydisperse and poor surface quality. The applied voltage ranged from 2–5 V depending on the cell resistance during deposition, Although the process takes place in fixed conditions of electrochemical deposition was performed under (galvanostatic/potentiostatic) conditions.

Table 1. Materials used for the electrochemical deposition of Ag NPs include $AgNO_3$ and KNO_3 (CDH-India), along with additional operating conditions.

Chemicals		PVP	PVA	Glycerin
$AgNO_3$	1g/100 mL	1g/1000 mL used 10 mL	1g/1000 mL used 10 mL	1g/1000 mL used 10 mL
KNO_3	0.03g/100 mL	PH=7	PH=7	PH=7
D. w.	0.75 µS/cm	0.75 µS/cm	0.75 µS/cm	0.75 µS/cm
Temperature	30-40 °C	30-40 °C	30-40 °C	30-40 °C
Total current density	500 A/m_2	500 A/m_2	500A/m_2	500 A/m_2
Anode Size (graphite)	12 cm_2	12 cm_2	12 cm_2	12 cm_2
Anode current intensity	0.60 A	0.60 A	0.60 A	0.60 A
Time of voltage	(V)/(min)	7.5 (V)/60 (min)	8.7 (V)/60(min)	8.5 (V) /60 (min)

Source: Elaborated by the authors.

3. Results and discussion

The AFM analysis of the electrogenerated and precipitated Ag NPs (**Table 2**) reveals a root mean square (RMS) roughness of 17.7 nm. Samples stabilized with PVA show higher surface roughness than those with PVP and glycerin. The roughness profile is as follows: PVA > PVP > glycerin. Surface skewness (Ssk) is positive for both PVA and samples without stabilizers, indicating that the surface has more peaks than valleys. Additionally, the surface kurtosis (Sku) for all three samples is less than 3, confirming that they are platykurtic. Notably, the sample with glycerin is closest to 3 ≈ (2.32). The AFM analysis provides key topographical input about the surface morphology of the synthesized Ag nanoparticles. As exhibited in **Table 2**, when PVA was utilized as the stabilizing operator, the average surface

roughness (Ra) was the highest (~15.3 nm), suggesting a more irregular surface structure. PVP and glycerol-stabilized samples show the lowest roughness account (Ra~1.41 nm and ~0.708 nm, respectively), indicating a more uniform and smoother nanoparticle layer. Furthermore, the modified data in Table 3 shows the nanoparticle diameter in the PVP ~73.58 nm, for the PVA ~60.51nm and GLY ~60.64 nm. As for the specimen that did not employ any stabilizer, the size of the nanoparticles was ~65.92 nm. These results suggest that PVA acted as a more effective stabilizer. is better than the other two stabilizers, the PVP and GLY., and the destabilized sample.

Table 2. Atomic force microscopy dimensions of Ag NPs precipitate particles from the ($AgNO_3$+KNO_3) suspension.

Photography surface roughness test - CSPM				
Amplitude parameters				
Ag	Without GLY PVP, PVA	PVP	PVA	GLYSERIN
Roughness average (Ra) (nm)	9.82	1.41	15.3	0.708
Root mean square (sq) (nm)	11.3	1.66	17.7	0.858
Surface kurtosis (sku) (nm)	1.8	2.04	1.8	2.32
Peak-peak (sy) (nm)	39.3	6.38	61.3	3.92
Ten-point height (sz) (nm)	39.2	3.65	61.2	3.87
Hybrid parameters				
(mean summit curvature) Ssc [1/nm]	−0.037	−1	−0.133	−0.0067
partition middle square slope (sdq) [1/nm]	0.777	0.118	1.44	0.067
Surface area ratio (sdr)	23.3	0.678	63.6	0.223
Functional parameters				
Surface bearing index (sbi)	5.58	5.11	5.58	0.954
Core fluid retention index (sci)	1.49	1.38	1.49	1.5
valley fluid retention index (svi)	0.0691	0.107	0.0692	0.105
Reduced summit height (spk) (nm)	4.18	0.101	6.53	0.547
Core roughness depth (sk) (nm)	34.2	5.06	53.3	2.4
Reduced valley depth (svk) (nm)	0.997	1.19	1.56	0.613
Spatial parameters				
(density of summits) Sds [1/um^2]	242	0	269	274
Fractal Dimension	2.61	2.47	2.6	2.73
Avg. Diameter (nm)	65.92	73.58	60.51	60.64
Voltage (V)	8.7	9.3	7.5	8.5

Source: Elaborated by the authors.

Table 3. Atomic force microscopy (AFM) parameters for Ag NPs electrochemical deposition from the ($AgNO_3$ + KNO_3) suspension: cumulative percentage and average particle size distribution (nm).

Metal oxide Ag	Diameter (nm)	Cumulation (%)	Average distribution (nm)	2-dimension distribution X,Y (nm)	3-dimension distribution X,Y,Z Z=high of peak (nm)
PVP	50-105	50-100	73.58	6.00	6.29
PVA	10-175	10-100	60.51	60.00	60.39
glycerin	40-125	40-100	60.64	3.92	3.92
Without PVP, PVA, GLY	35-145	35-100	65.92	38.62	38.62

Source: Elaborated by the authors.

The study utilized atomic force microscopy (AFM) to examine Ag NPs synthesized through an electrochemical process, utilizing PVA, PVP, and glycerin as stabilizers. The particle size of Ag when using 10 mL of PVP as a stabilizer is illustrated in Fig. 1a. The dark dots of the figure represent the distribution of metal particles, while the light points indicate the distance between the nanoparticles, which is approximately 6 nm. Figure 1b displays the spatial distribution of metal oxide in three dimensions (X, Y, Z) (Gadelmawla *et al.*, 2002). Here, (X, Y) represents the spatial area, and (Z=6.29 nm) indicates the elevation, which falls within the nanoscale range (0-100 nm). Additionally, Fig. 1c shows the particle size distribution of silver nanoparticles ranging from 50-105 nm. The average cumulative granularity distribution of particle distances for Ag NPs, when using 10 mL of PVP, was found to be 73.58 nm. The parameters are also represented in Fig. 2, Fig. 3 (average particle size: 60.64 nm) and Fig. 4 (average particle size: 65.92 nm), as well as in Table 3 above, where it is evident that the sample prepared with PVP exhibits better performance compared to those prepared with glycerin and PVA (PVP > Glycerin > PVA).

https://doi.org/10.26850/1678-4618.eq.v51.2026.e1546

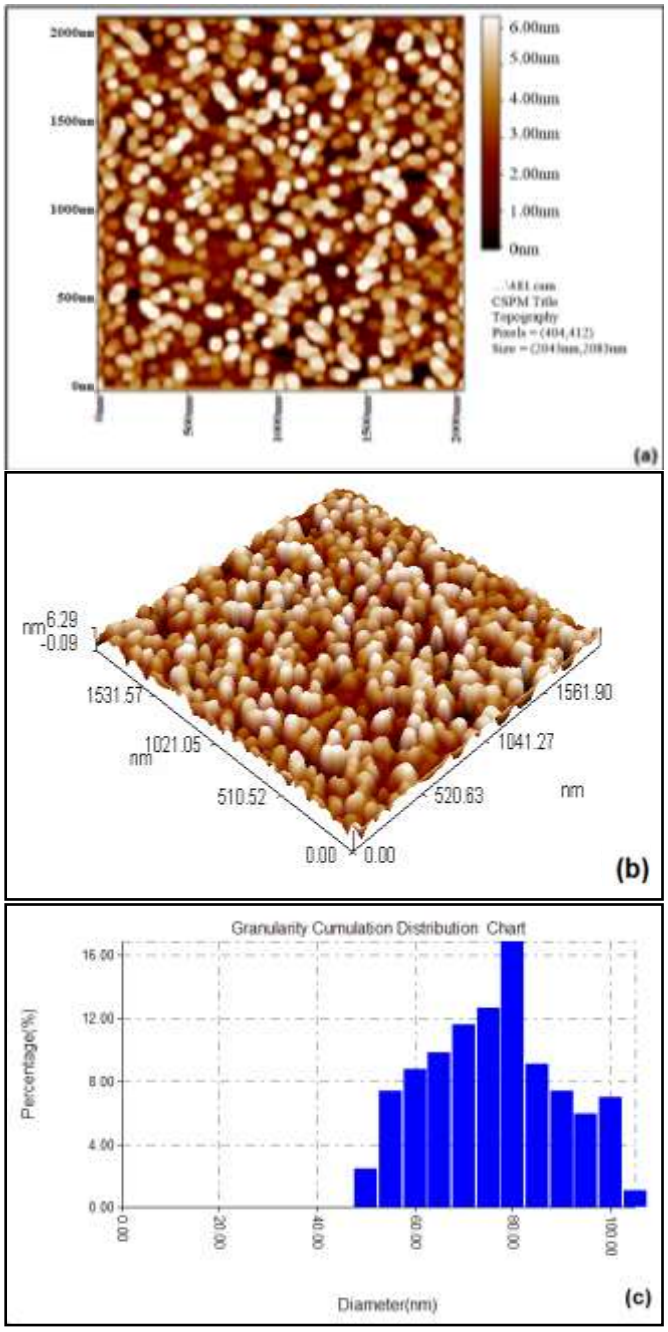

Figure 1. Atomic force microscopy (AFM) images of Ag NPs obtained by electrochemical sedimentation from an ($AgNO_3$ + KNO_3) suspension with (10 mL) PVP. Average particle size: 73.58 nm **(a)** 2-distance photo, **(b)** 3-Size photo, **(c)** Granularity cumulation division scheme.
Source: Elaborated by the authors.

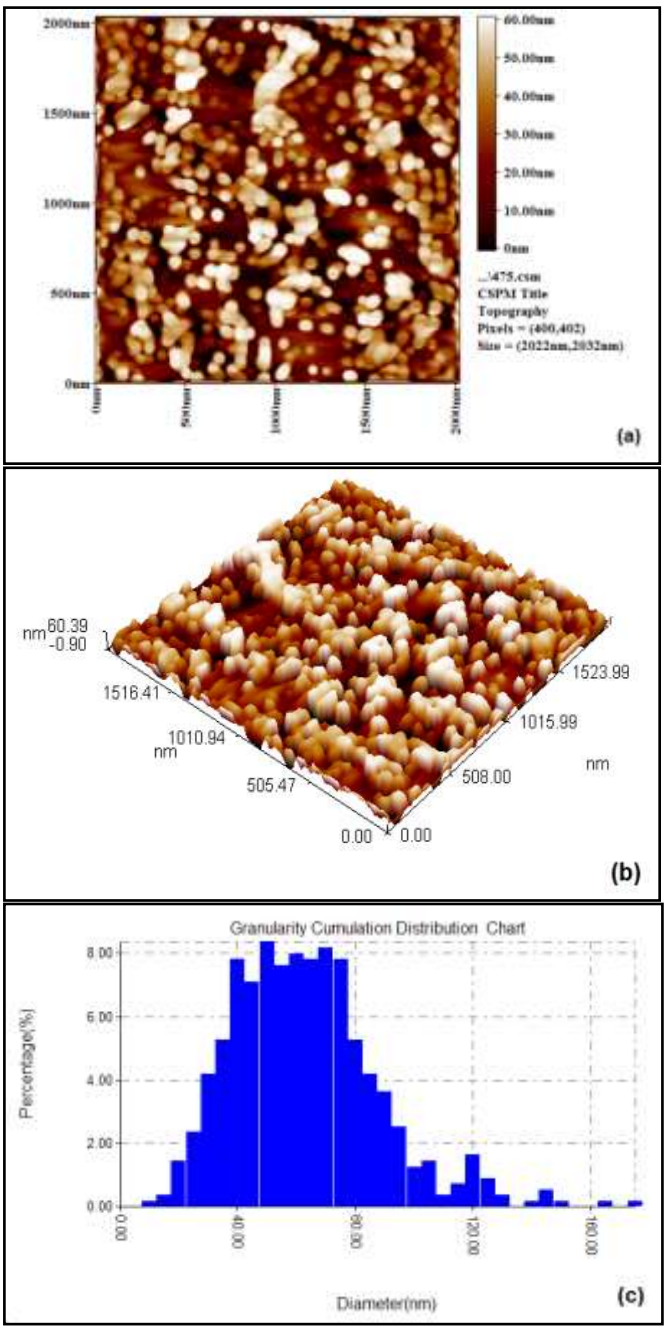

Figure 2. Atomic force microscopy (AFM) images of Ag NPs obtained by electrochemical sedimentation from an ($AgNO_3$ + KNO_3) suspension with (10 mL) PVA. Average particle size: 60.51 nm **(a)** 2-Size photo, **(b)** 3-Size photo, **(c)** Granularity cumulation division scheme.
Source: Elaborated by the authors.

https://doi.org/10.26850/1678-4618.eq.v51.2026.e1546

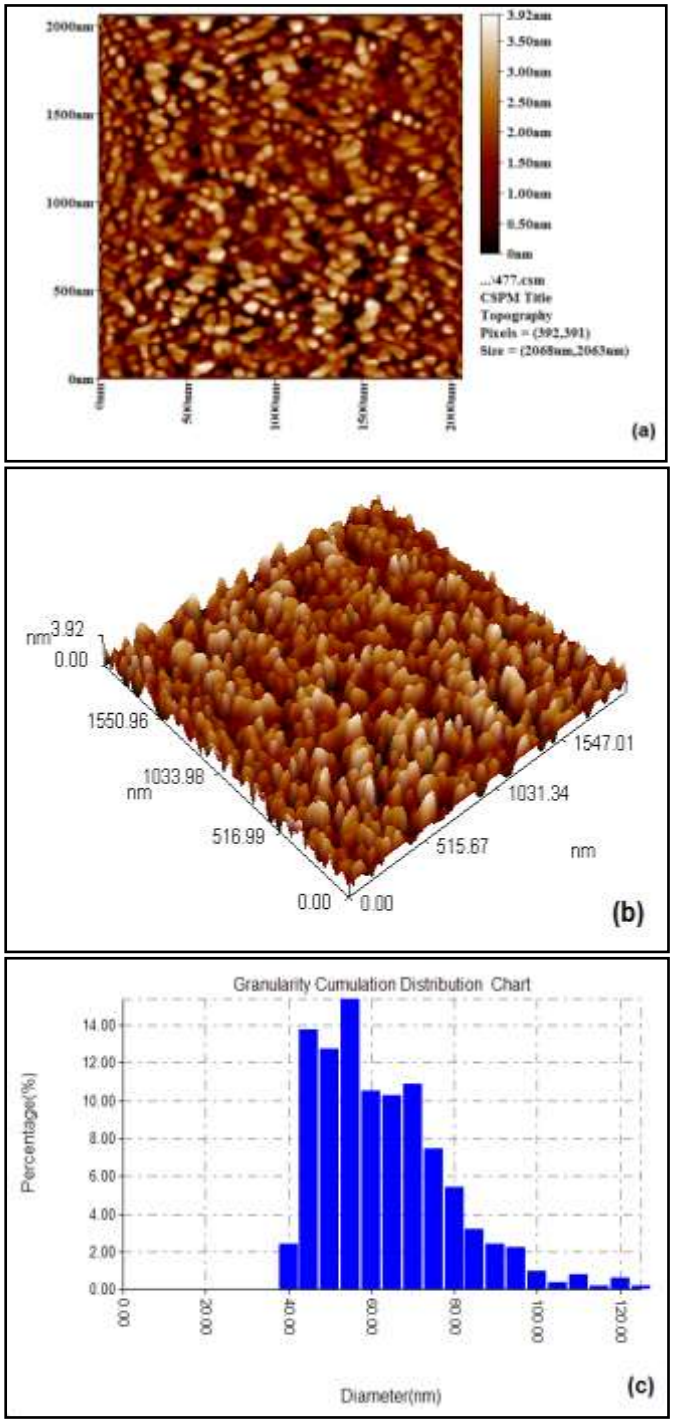

Figure 3. Atomic force microscopy (AFM) images of Ag NPs obtained by electrochemical sedimentation of ($AgNO_3$ + KNO_3) suspension by (10 mL) glycerin. Average particle size: 60.64 nm **(a)** 2-Size photo, **(b)** 3-Size photo, **(c)** Granularity cumulation division scheme.
Source: Elaborated by the authors.

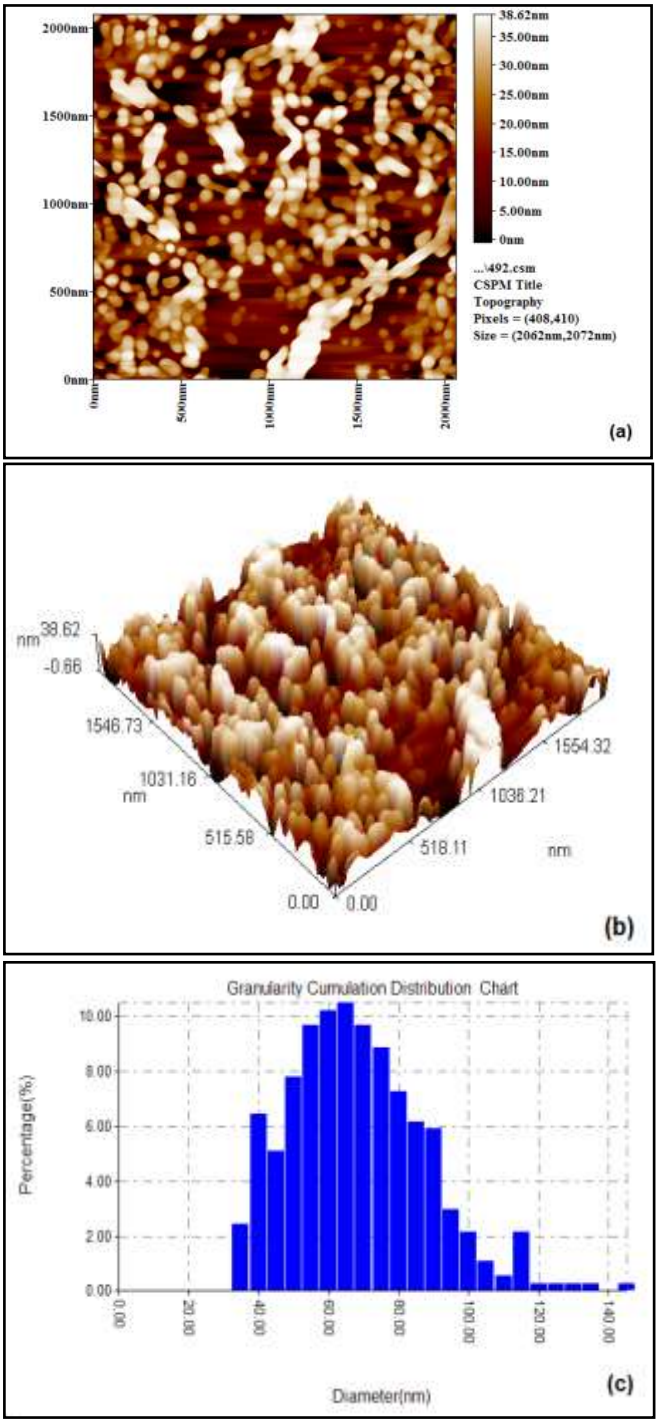

Figure 4. Atomic force microscopy (AFM) images of Ag NPs obtained by electrochemical sedimentation of ($AgNO_3$ + KNO_3) solution without additional stabilizers. Average particle size: 65.92 nm **(a)** 2-Size photo, **(b)** 3-Size photo, **(c)** granularity cumulation division scheme.
Source: Elaborated by the authors.

3.1. X-ray dimension of Ag NPs electrochemical sedimentation

To define the crystalline state of silver, were analyzed the silver nanopowder using XRD, based on its distinguishing face-centered cubic (fcc) structure (Buendía-Otero *et al.*, 2022). This analysis reflects the crystal nature of the atomic silver powder NPs. The silver NPs were obtained from the deposit of silver in an aqueous suspension, followed by calcination at 300 °C to eliminate impurities, increase surface area, remove residual organic compounds and physically adsorbed water. While this process helps improve nanoparticle purity and crystallinity, it does not remove metallic impurities or non-volatile ash, which may remain in the final product. The results align with the face-centered cubic structure. The diffractogram displays three distinct peaks within the 2θ range of 30-80° (specifically at 2θ = 38°, 45°,

65°), corresponding to the planes (111), (200) and (220) (Ponsanti *et al.*, 2020). These reflections confirm the face-centered cubic structure of metallic silver, as established in prior microstructure analysis. Notably, the peak at 38° shows a higher intensity than at 45° and 65°. This indicates that the silver NPs have an optimal atomic arrangement along the (111) plane, consistent with findings by (JCPDS file nos. 84-0713 and 04-0783) (Wang *et al.*, 2015). Such arrangements suggest a strong response of silver NPs due to a higher intensity of atoms on the (111) plane. The Debye-Scherrer equation (**Eq. 1**) was employed to calculate the average crystal size, assuming the crystal lattice is defect-free (Rabiei, 2020).

$$D = \frac{k \cdot \lambda}{FWHM \cdot \cos\theta} \quad (1)$$

where D: average crystal size, K: shape factor (0.9), λ: wavelength of the X-ray beam ($\lambda_{Cu\text{-}K\alpha}$ = 1.54178 A° x $10^{-10}m$), θ: Bragg diffraction angle, FWHM: full widths at half maximum of the diffraction peak.

Using Origin Pro 2020b software, the width of the prominent peaks was determined by fitting multiple peak adjustments, as shown in **Table 4**. Four prominent diffraction peaks were observed between 20 and 80° at 38.45°, 44. 48°, 64.69°, and 77.62°. corresponding to the (111), (200), (220), and (311) planes of silver, respectively. These results confirm the complete reduction of $AgNO_3$. The particle size was further validated using the Debye-Scherrer equation, yielding a value of 46.64 nm. This result closely aligns with the average crystal size derived from the XRD pattern. The results show good agreement when compared with the high-resolution transmission electron microscopy HRTEM analysis, which estimated an average particle size of approximately 40 nm (Annamalai and Nallamuthu, 2016). In the fragment grain boundary analysis, the particle size results obtained from HRTEM and the Debye-Scherrer method differed by less than 6%, within an acceptable margin of error (Shuaib *et al.*, 2020). As shown in **Fig. 5**. This consistency further validates and reliability of the measurements in this study. The Ag particles, including (Ag) with detectable {111} planes, were shown to be more active in photocatalytic reactions compared to particles containing {100} planes (Ho and Huang, 2009; Kuo *et al.*, 2008; Lyu *et al.*, 2010).

Table 4. Grain size of Ag nanopowder (without stabilizer) obtained from the electrogeneration of ($AgNO_3$ + KNO_3) suspensions.

Terrible peak 2θ (degree)	hkl	Terrible peak θ (degree)	Terrible FWHM of peak (β) (radians)	Particle Size of the (D) (nm)	d-spacing (nm)
38.45	111	19.22	3.14×10^{-3}	46.64	0.23
44.48	200	22.24	6.10×10^{-3}	24.56	0.20
64.69	220	32.34	7.85×10^{-3}	20.89	0.14
77.62	311	38.81	7.89×10^{-3}	22.53	0.12

Source: Elaborated by the authors.

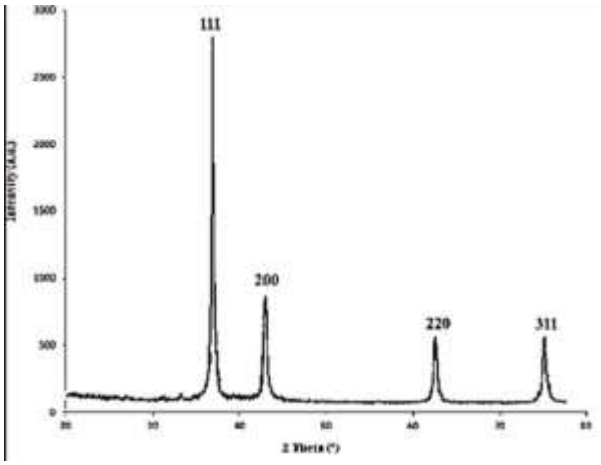

Figure 5. X-ray diffraction (XRD) pattern of Ag nanopowder (without stabilizer) obtained from the electrogeneration of ($AgNO_3$ + KNO_3) suspensions.
Source: Elaborated by the authors.

Figures 6-9 reveal the presence of pure silver through energy-dispersive spectroscopy EDS analysis of electrically prepared samples using two inert graphite electrodes as the anode and cathode. The electrolyte suspension consisted of $AgNO_3$ (1 g/100 mL), KNO_3 (0.03 g/100 mL), and 10 mL of glycerin. During electrolysis, the decomposition of the suspension led to the migration of negative ions toward the anode and positive ions toward the cathode. The use of stabilizers reduced ion migration, increased voltage, and decreased current density over time, enhancing the cathode surface coverage and lowering the reaction rate. When using 10 mL of glycerin or PVA as stabilizers, the size of the nanoparticles was reduced, forming uniform spherical shapes with varying sizes depending on ion migration. A higher concentration of stabilizers resulted in smaller nanoparticles. This indicates that the stabilizer remained unchanged during the process, the result of the high voltage and the elevated temperature (Sati *et al.*, 2025). Poly N-vinylpyrrolidone, PVP, was utilized as a stabilizer to suspend Ag NPs, significantly increasing the average size of silver powder and reducing the sedimentation rate. To manufacture silver nanoparticles, controlling the electrical parameters was necessary to regulate the particle size during the electro-reduction of silver ions. Parameters for the electrogeneration of Ag NPs from $AgNO_3$ suspensions using different stabilizers, including PVP, PVA, and glycerin are in **Table 5**. The product showed that the transfer of the charge from the silver clusters installed with PVP from the Cathodic area into the bulk of the suspension played a decisive role in the formation of polydisperse. PVP also had a fundamental role in accelerating the formation of silver particles while reducing sedimentation on the surface of the cathode. Electrochemical synthesis proved to be an effective method for preparing nanoparticles on a large scale, particularly noble metals like silver, platinum, and gold, under static conditions. During the electrolysis, the PVP-containing electrolyte gradually changed color from light yellow to dark yellow and, ultimately, gray silver nanoparticles formed. The yellow color indicated the genesis of silver nanoparticles, while the cathode became slightly black at the experiment's conclusion (Rodriguez-Sanchez *et al.*, 2000; Yin *et al.*, 2003). The PVC stabilization mechanism during the electrochemical synthesis of silver molecules relies on its structural properties. The PVP has a polyvinyl backbone with polar groups that coordinate with silver ions to form Agn^{n+}-PVP complexes (where n indicates the number of silver ions). This process involves the coordination of PVP with

silver ions: coordinative bonds form between PVP and Agn^{n+}, resulting in Agn^{n+}-PVP complexes. And the electrochemical reduction of Ag^{n+}-PVP at the cathode generates silver atoms (Agn^{O}–PVP), stabilized by (PVP). The C-N and C=O groups in PVP provide greater electronic density to the silver ions than water, enabling the Ag^{n+}–PVP complex to gain electrons more readily than Ag^{+}-H_2O complexes. This stabilization prevents silver sedimentation and promotes polydisperse nanoparticles by limiting nucleation and aggregation. Experiments showed that the suspension color around the cathode transitioned from yellow to gray as silver ions were reduced. Without PVP, gray deposits appeared on the cathode, indicating the unregulated growth of silver particles. Zhang *et al*. (1996) demonstrated that PVP's steric effect prevented particle aggregation and promoted the formation of polydisperse silver nanoparticles. Large particles were washed with water and ethanol three consecutive times, centrifuged, and redispersed in ethanol. The Ag particles strongly adsorbed PVA. This electrochemical method is effective, straightforward, and highly productive for synthesizing spherical silver nanoparticles in an aqueous suspension without membrane media. This study obtained silver NPs from the electrolyte (potassium nitrate) rather than a sacrificial anode. PVA hydrophilic properties interacted with water, stabilizing silver nanoparticles in suspension. This method offers several advantages, including simplicity, high productivity, excellent particle dispersion, stability, precise size control, and minimal byproducts, making it highly effective for future applications in metal synthesis and nanoparticle manufacturing. From the collection of topographic forms from the field-emission scanning electron microscopy FESEM, it was observed that some particles had dendritic or polydisperse shapes in addition to spherical ones, except for the method using PVA as the stabilizer, which resulted in entirely spherical particles with small nanoparticles size. That is in spherical shape and is characterized by a small nanoparticle size 60.51 nm. Variety in size and shapes is attributed to the insufficiency or absence of stabilizers, that allows the silver nanoparticles more freedom, which enhances the dendritic or polydisperse structures. From this standpoint, the nanoparticles of the prepared silver by adding PVA, which have a wide surface area for possessing the spherical particles and the small nano size, qualify them to be highly effective in the photodegradation process.

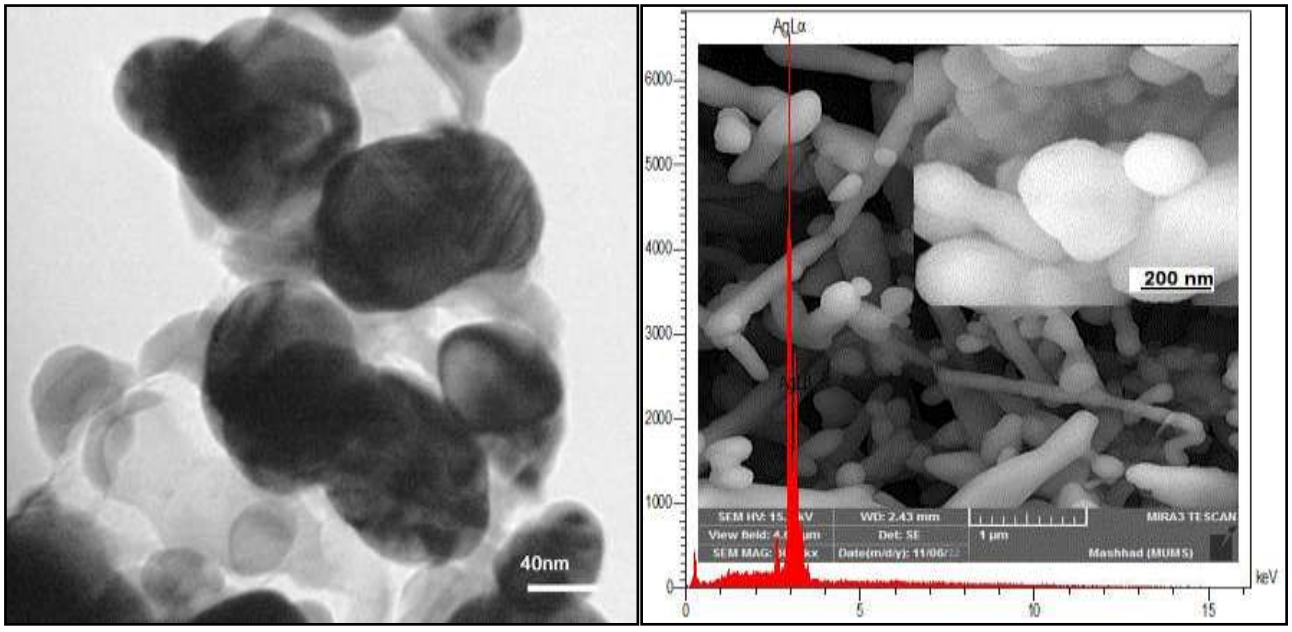

(a) **(b)**

Figure 6. TEM and SEM images and EDS analysis of electrochemically deposited Ag NPs obtained using potassium nitrate with 10 mL of glycerin under vigorous stirring. The FESEM, HRTEM, and EDS results confirmed that the sample consists of 100 wt.% and 100 at.% Ag. **(a)** HRTEM image illustrating the nanoscale particle size 40 nm, and morphology of the Ag nanoparticles. **(b)** FESEM image showing the surface morphology and dendritic or polydisperse shapes distribution of Ag nanoparticles.
Source: Elaborated by the authors.

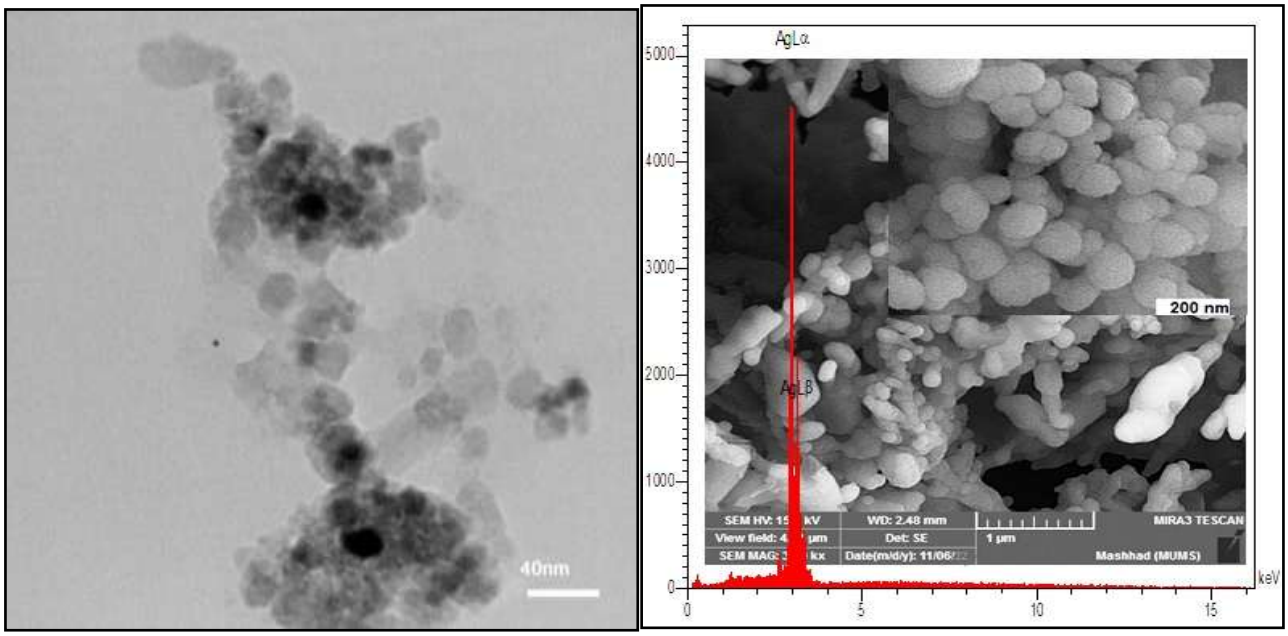

(a) (b)

Figure 7. TEM and SEM images and EDS analysis of electrochemical deposited Ag NPs obtained using potassium nitrate with 10 mL of PVA, with vigorous stirring. The content in FESEM, HRTEM, and EDS electrochemical deposition of Ag NPs using potassium nitrate with 10 mL of PVA, under vigorous stirring. The content obtained in FESEM, HRTEM, and EDS shows a weight and atomic weight of 100 wt% of Ag. **(a)** HRTEM image illustrating the nanoscale particle size 40 nm, and morphology of the Ag nanoparticles. **(b)** FESEM image showing the surface morphology and entirely spherical particles with small distribution of Ag nanoparticles.
Source: Elaborated by the authors.

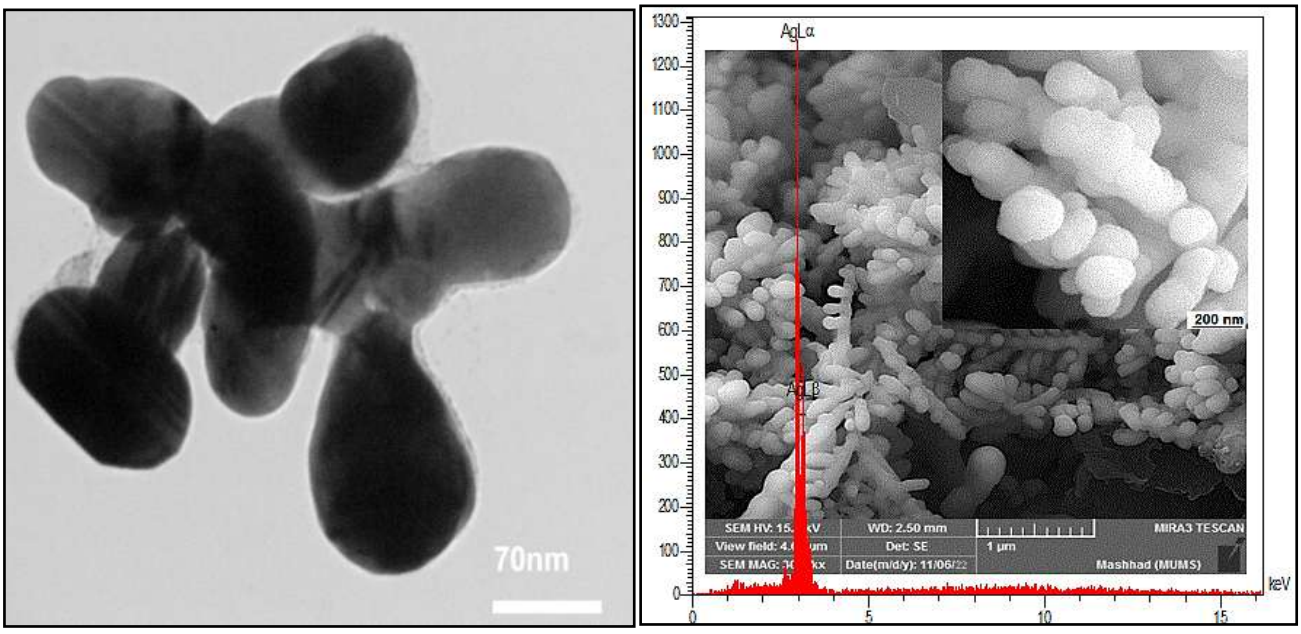

(a) (b)

Figure 8. TEM and SEM images and EDS analysis of electrochemical deposited Ag NPs obtained using potassium nitrate with 10 mL PVP, with vigorous stirring. The content obtained in FESEM, HRTEM and EDS shows weight and atomic weight% 100 of Ag. **(a)** HRTEM image illustrating the nanoscale particle size 70 nm, and morphology of the Ag nanoparticles. **(b)** FESEM image showing the surface morphology and dendritic or polydisperse shapes distribution of Ag nanoparticles.
Source: Elaborated by the authors.

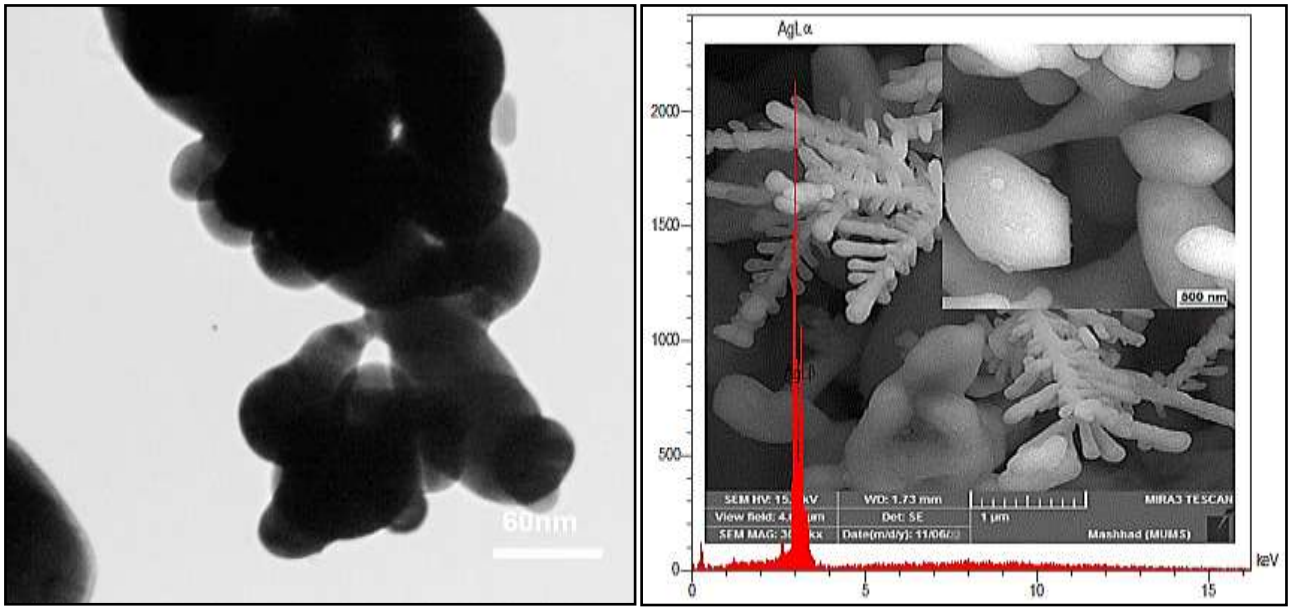

(a) (b)

Figure 9. TEM and SEM images and EDS analysis of electrochemical deposited Ag NPs obtained using potassium nitrate without stabilizer, with vigorous stirring. The content obtained in FESEM, HRTEM and EDS show weight and atomic weight %100 of Ag. **(a)** HRTEM image illustrating the nanoscale particle size 60 nm, and morphology of the Ag nanoparticles. **(b)** FESEM image showing the surface morphology and dendritic or polydisperse shapes distribution of Ag nanoparticles.
Source: Elaborated by the authors.

Table 5. Parameters for the electrogeneration of Ag NPs from $AgNO_3$ suspensions using different stabilizers, including PVP, PVA, and glycerin.

Stabilizer	Ag (wt. %)	Voltaic (V)	HRTEM (nm)	AFM Average size diameter (nm)
GLY	100	8.5	40	60.64
PVA	100	7.5	40	60.51
PVP	100	9.3	70	73.58
without	100	8.7	60	65.92

Source: Elaborated by the authors.

Photodegradation of methylene blue dye using Ag standard and Ag prepared, silver nanoparticles prepared in the presence of the stabilizer PVA chosen to use as a catalyst in photodegradation, due to their large surface area and a small particle size of about 60.51 nm after calcination at 300 °C as catalysts. methylene blue. It is also known as 3,7-bis(dimethylamino)-phenothiazin-5-ium chloride, which is a salt widely used as both a dye and as a medicine. It treats methemoglobinemia by chemically reducing ferric iron to ferrous iron in hemoglobin (Mirsalari and Nezamzadeh-Ejhieh, 2020; Tkach *et al.*, 2020). Historically, MB has been used to manage cases where methemoglobin levels exceed 30% or when oxygen therapy is insufficient (Ahmad and Aqil, 2008). Methylene blue MB was first discovered in 1876 by Heinrich Caro. The World Health Organization has included it on its list of essential medicines (WHO, 2019). Methylene blue has numerous medical applications. It is one of the oldest antimalarial agents and was tested for this purpose in the late 19 th century (Shanks, 2012). It has been specifically used alongside amodiaquine and has shown efficacy in treating *Plasmodium falciparum* malaria, particularly in African adults and children (Bosoy *et al.*, 2008; Shanks, 2012). MB is also used to treat methemoglobinemia (a condition where an abnormal level of methemoglobin is produced in the blood) in children and adults (Stewart and Christopher, 2014). Clinical applications of methylene blue include treating low blood pressure (hypotension) associated with various conditions and addressing hypoxia and hyperdynamic circulation linked to liver cirrhosis (Chaluvaraju *et al.*, 2022). In the current study, methylene blue (MB), was selected as a basic dye due to its properties as a basic dye with excellent water solubility. The standard Ag NPs (99%) were purchased from Fluka, Switzerland. A homemade photoreactor was equipped with a Philips mercury bulb (250 W) with the glass sheath removed to serve as the UV light source. A Shimadzu UV-Vis spectrophotometer (Model 1876 PC Japan) was used to measure the MB dye solutions' degree of degradation. The reactor setup included an airless system to maintain a constant temperature and electric stirring, using a hot plate (LAB Tech, made in Korea). The UV lamp was positioned vertically, focusing on a 15 cm area of the solution. The experiments were conducted at 25 °C. The pH of the suspension was adjusted to 0.01 Eq./L NaOH or 0.01 mol/L HNO_3, measured with Hanna pH meter. During the experiment, magnetic stirring ensured uniform mixing of the solution. The solution was irradiated with UV light for specific time intervals. Samples were withdrawn using a syringe and filtered via centrifuge (ALL-PRO, 4000 rpm, 10 min). Floating materials were separated using a syringe, and the sample was re-centrifuged for the same duration. The absorption of the filtered samples was measured using the UV–Vis spectrometer. The color removal and degradation rate, indicated by intensity changes at the dye maximum wavelength (λ_{max}), were analyzed using the Langmuir-Hinshelwood relationship. After the photoirradiation process, the decomposition efficiency (%) was calculated as the efficiency (%). The degradation of methylene blue was assessed using the following equation, which quantifies the reduction of the dye (**Eq. 2**): **Photodegradation Efficiency (P.D.E) = (D%).**

$$(D\%) = \left[\frac{C_0 - C_a}{C_0}\right] \times 100\ (\%) \qquad (2)$$

where the degradation rate is denoted by D%; the initial concentration of dye solution is represented by C_o, and the effectiveness of the catalyst in stimulating the adsorption of dye concentrations C_a.

https://doi.org/10.26850/1678-4618.eq.v51.2026.e1546

3.2. In the absence of UV radiation of the silver catalyst (dark response)

The test was conducted without UV radiation, simulating the dark response using Ag NPs as the catalyst. The results are shown in Fig. 10. Without ultraviolet radiation, no significant degradation of the dye concentration occurred in the dark when the catalyst was added. During the incubation period, the initial dye concentration decreased, but after a short time, it stabilized due to the formation of a monolayer on the catalyst surface. Equilibrium was reached after 120 min. The decomposition efficiency was calculated as 90.3% for the Ag standard and 80.8% for the as-prepared Ag NPs (calcined at 300 °C).

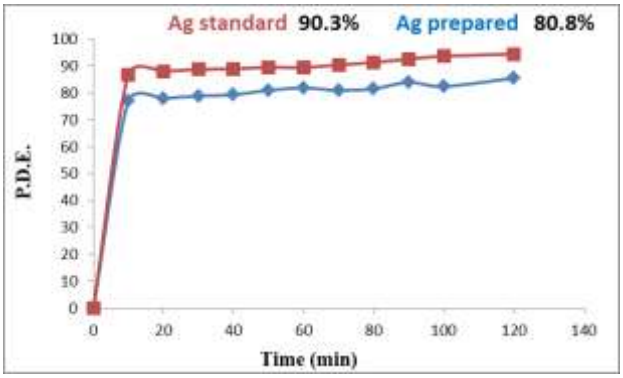

Figure 10. Decay efficiency of MB dye in the absence of UV radiation.
Source: Elaborated by the authors.

3.3. Photodegradation of MB solution under UV light without a catalyst

During the photoreaction of the MB solution, reactions occurred in the presence of UV light but without an Ag catalyst, as shown in Fig. 11. The photodegradation efficiency was 50.4% after 120 min of UV treatment without the catalyst. The Tauc plot in Fig. 11. kept as is that the electron transfer from the conduction band to the valence band minor recording retained, band gap energy 1.8 eV.

3.4. The influence of catalyst mass

The effect of Ag NPS was studied on the photocatalytic degradation of (MB). The solution has been analyzed under operational conditions that included: a 4-ppm dye concentration, the light intensity of 250 W, and a temperature of 25 °C, using varying amounts of nanoparticles (commercial and prepared) ranging from 0.01 to 0.07 g. The results, shown in the Fig. 12, showed that the degradation rate increases with the catalyst mass to a certain point, after which efficiency plateaued is proven and then begins with slight decrease in the higher catalyst dosages The optimum catalyst mass was determined at 0.03 gram for each of the standard and prepared catalyst mass, as the efficiency of photocatalytic degradation reached 94.6% and 91.72%, respectively.

The influence of pH variation (ranging from 2 to 10) was also studied under constant operational conditions, including a dye concentration of 4 ppm, light intensity of 250 W, Ag catalyst dose of 0.03 g, and a temperature of 25 °C. The results are shown in Fig. 13.

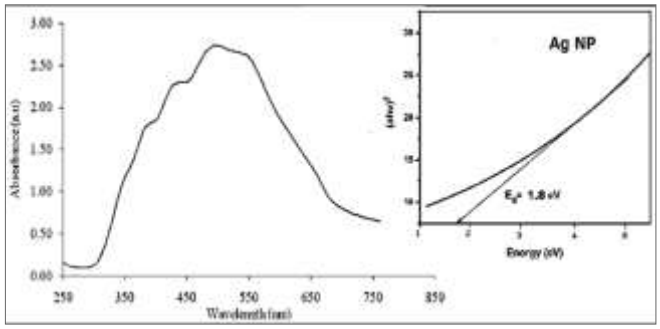

(a)

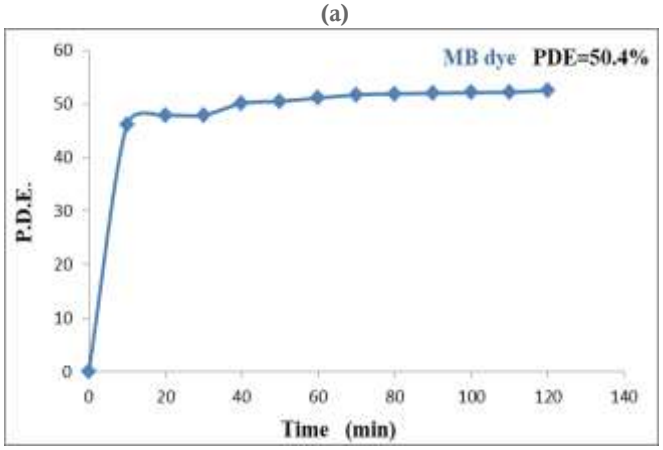

(b)

Figure 11. Photodegradation efficiency of MB dye in the absence of a catalyst and measurement of the energy bandgap of Ag NPs using UV light (Mega 2100 Double-Beam UV–Vis spectrophotometer). **(a)** Optical bandgap determination of Ag NPs from the UV–Vis absorption spectrum. **(b)** Photodegradation of MB dye without a catalyst under UV irradiation.
Source: Elaborated by the authors.

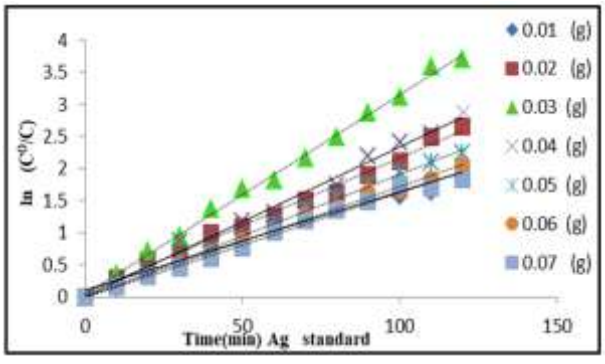

(a)

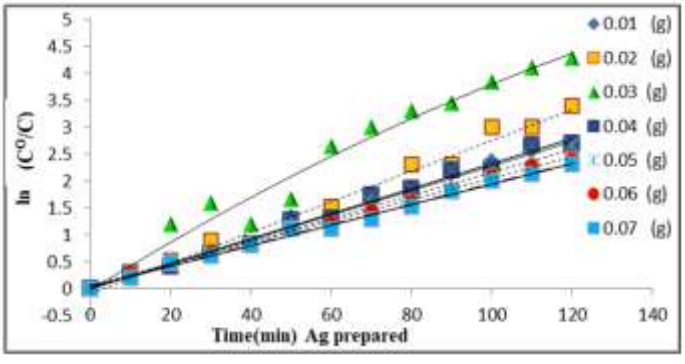

(b)

Figure 12. Influence of the mass of **(a)** standard silver NPs and **(b)** prepared silver NPs on the efficiency of MB photodegradation.
Source: Elaborated by the authors.

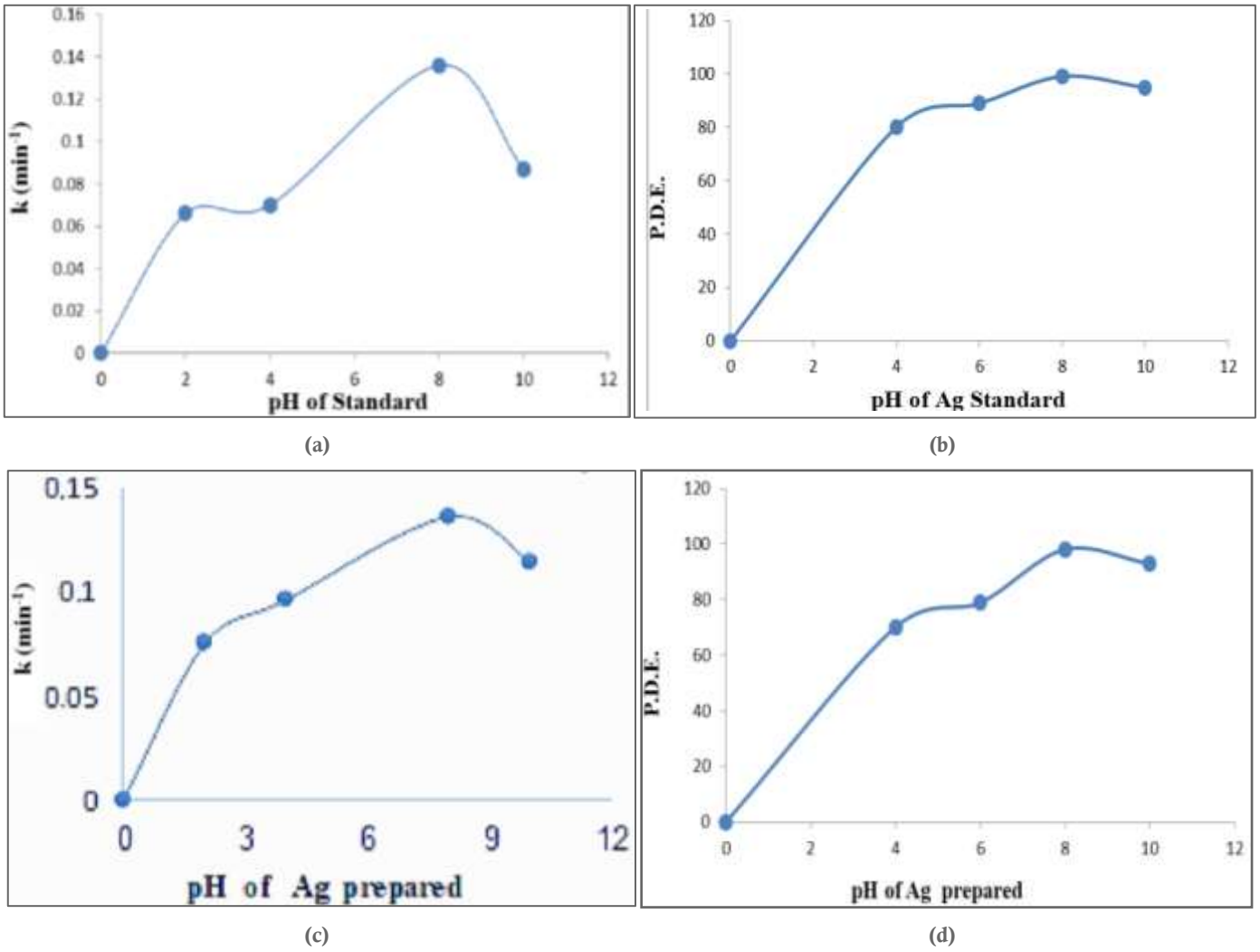

Figure 13. Effect of pH on the photolytic activity of MB using 0.03 g of Ag NPs **(a)** Pseudo-first-order rate constant (k) of MB photodegradation using 0.03 g of standard Ag NPs at different pH values. **(b)** Photodegradation efficiency of MB using 0.03 g of standard Ag NPs at different pH values. **(c)** Pseudo-first-order rate constant (k) of MB photodegradation using 0.03 g of prepared Ag NPs at different pH values **(d)** Photodegradation efficiency of MB using 0.03 g of prepared Ag NPs at different pH values.
Source: Elaborated by the authors.

The effect of pH on the degradation efficiency of 0.03 g of Ag NPs was investigated based on the point of zero charge (pH_pzc). The pH values were adjusted in the range of 2 to 10. Maximum degradation was observed at pH 8, achieving photodegradation efficiencies of 98.6% for standard Ag NPs and 95.7% for prepared Ag NPs. The elevated photodegradation of methylene blue in basic media might be due to the enhanced generation of hydroxyl radicals (•OH). These hydroxyl radicals are strong oxidizing agents, which are responsible for the higher degradation rate at higher pH levels. Although complete decolorization is rare, some degradation may still occur under these unfavorable conditions. In our experiments, MB under extreme acidity conditions was below the detection threshold for reliable kinetic analysis; therefore, it was negligible.

3.5. Effect of initial concentration of dye (Mb)

Under constant working conditions, the initial dye concentrations were evaluated based on the percentage of photodegradation activity. The experimental parameters included a light intensity of 250 W, an Ag catalyst dose of 0.03 g, pH = 8, temperature = 25 °C and the variable dye concentration ranging from 1 to 7 ppm, as shown in **Fig. 14**. An increased rate of photolysis activity was observed at lower initial dye concentrations due to the higher adsorption of dye molecules onto the catalyst surface. However, the interaction between dye molecules and hydroxyl radicals was decreased at higher dye concentrations due to a scavenging effect caused by the excess molecules. This resulted in the absence of a direct relationship between dye and reactive species (Munesh, 2012).

Figure 15 show the effect of temperature on the photolytic activity of MB using 0.03 g of standard and prepared Ag NPs, while **Fig. 16** presents the Arrhenius plots for standard and prepared Ag NPs.

Table 6 shows the estimated rate constants, thermodynamic parameters and kinetic data for MB photodegradation between 303 K and 318 K using standard and prepared Ag NPs.

https://doi.org/10.26850/1678-4618.eq.v51.2026.e1546

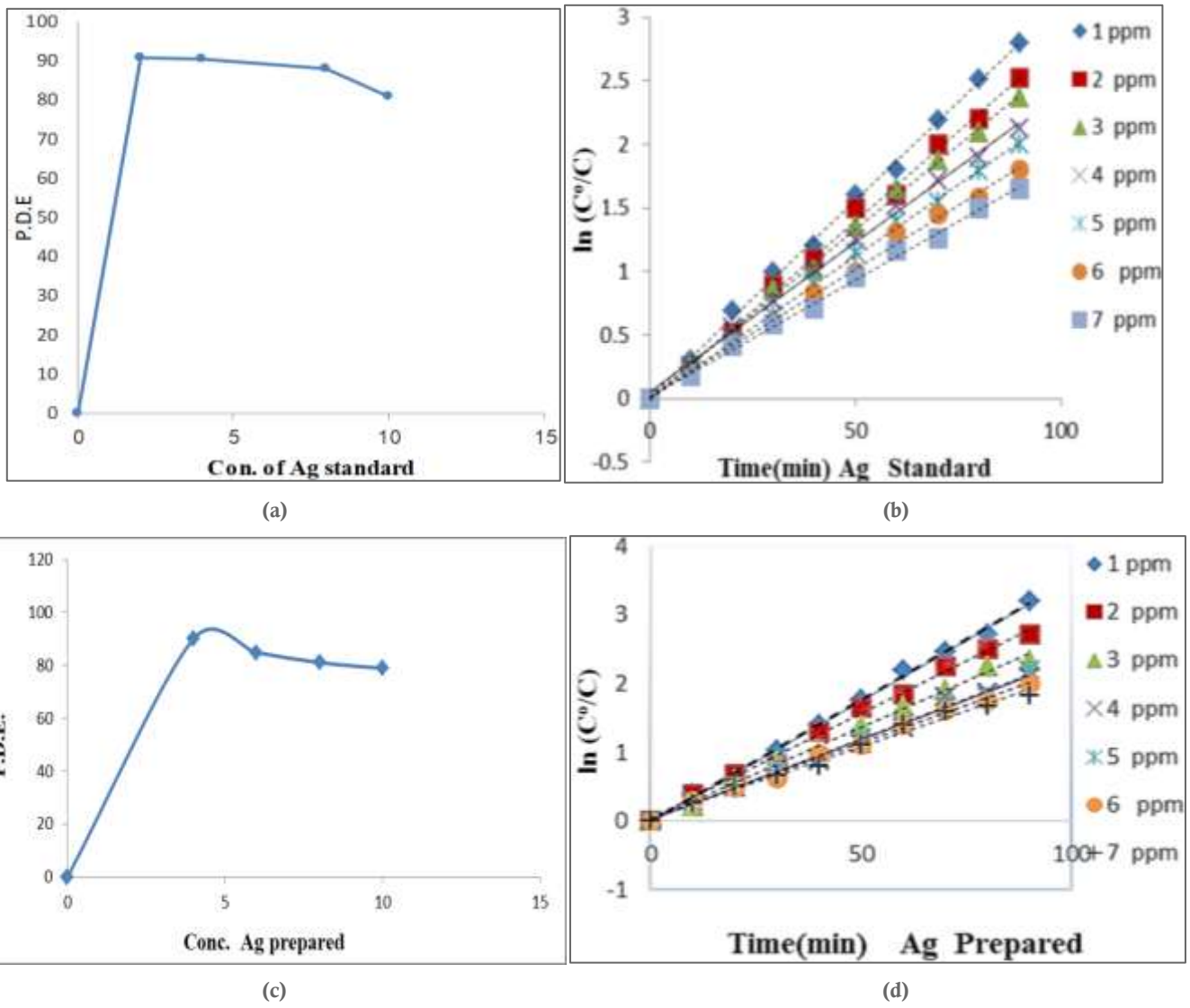

Figure 14. Photocatalytic degradation Efficiency of MB at varying dye concentrations using 0.03 g of Ag NPs **(a)** Photocatalytic degradation efficiency of MB at different initial dye concentrations using 0.03 g of standard Ag NPs. **(b)** Effect of the initial MB dye concentration on the photocatalytic degradation using 0.03 g of standard Ag NPs. **(c)** Photocatalytic degradation efficiency of MB at different initial dye concentrations using 0.03 g of prepared Ag NPs. **(d)** Effect of the initial MB dye concentration on the photocatalytic degradation using 0.03 g of prepared Ag NPs.
Source: Elaborated by the authors.

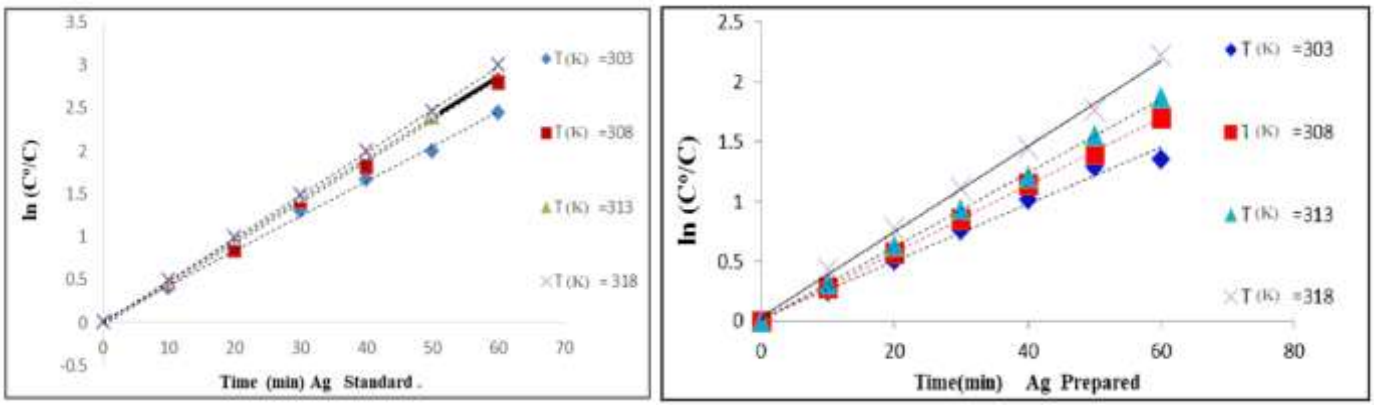

Figure 15. Effect of temperature on the photolytic activity of MB using 0.03 g of **(a)** standard Ag NPs and **(b)** prepared Ag NPs.
Source: Elaborated by the authors.

https://doi.org/10.26850/1678-4618.eq.v51.2026.e1546

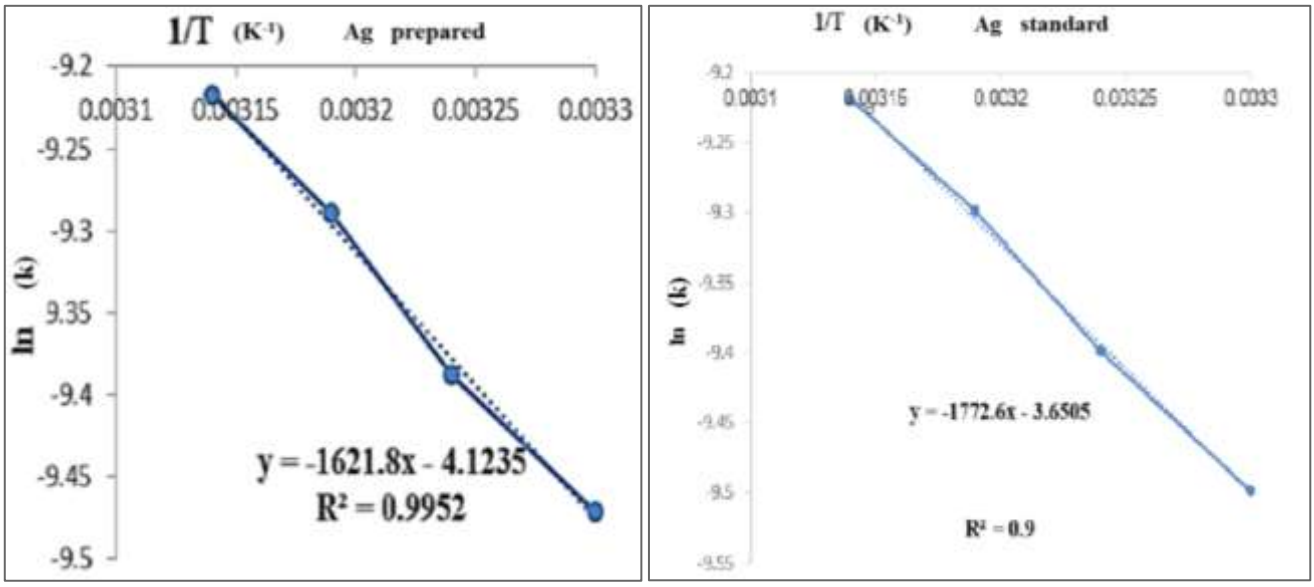

(a) (b)

Figure 16. (a) Arrhenius plot (ln k vs. 1/T) for MB photodegradation using 0.03 g of standard Ag NPs. **(b)** Arrhenius plot (ln k vs. 1/T) for MB photodegradation using 0.03 g of prepared Ag NPs. The activation energy (Ea) was calculated using the Arrhenius method by plotting ln (k) versus 1/T, with the slope equal to –Ea/R. The unit of Ea is correctly expressed as kJ mol^{-1}.
Source: Elaborated by the authors.

Table 6. Estimated rate constants, thermodynamic parameters, and kinetic data for MB photodegradation at (303-318) K using both standard and prepared Ag NPs.

T (K)		303	308	313	318
1\T (K^{-1})		0.00330	0.00324	0.00319	0.00314
k (sec^{-1}) ×10^{-5}	Ag prepared	76.977	8.372	9.243	9.923
	Ag typical	7.492	8.280	9.151	9.913
ln k	Ag prepared	−9.472	−9.388	−9.289	−9.218
	Ag typical	−9.499	−9.399	−9.299	−9.219
Ea (kJ mol^{-1})	Ag prepared		13.483		
	Ag typical		14.737		
$\Delta H^{o\#}$ (kJ mol^{-1})	Ag prepared	10.964	10.922	10.881	10.839
	Ag typical	12.218	12.176	12.135	12.093
$\Delta S^{o\#}$ (kJ mol^{-1} K^{-1})	Ag prepared		−0.279		
	Ag typical		−0.275		
$\Delta G^{o\#}$ (kJ mol^{-1})	Ag prepared	95.501	96.854	98.208	99.561
	Ag typical	95.543	96.876	98.210	99.543

Source: Elaborated by the authors.

3.6. The influence of temperature range

The thermodynamic parameters for the degradation of MB were evaluated. The positive $\Delta H^{o\#}$ indicates an endothermic interaction, while the positive $\Delta G^{o\#}$ reflects a non-spontaneous process. In our current method, the negative $\Delta S^{o\#}$ (**Table 6**) suggests the formation of a fully solvated structure consisting of dye molecules and intermediates, such as hydroxyl radicals. **Figure 17** shows the photosynthesis of silver under the conditions shown in **Table 6**.

Using silver nanoparticles, a mechanism for dye decomposition via photocatalysis is proposed as follows:

$$Ag + h\nu \rightarrow Ag^{+} + e^{-} \quad (3)$$

$$e^{-} + O_2 \rightarrow {}^{*}O_2^{-} \quad (4)$$

$$Ag^{+} \rightarrow Ag + h^{+} \quad (5)$$

$$h^{+} + H_2O, OH^{-} \rightarrow {}^{*}OH \quad (6)$$

$$MB^{+} + OH^{*} \rightarrow \text{Degradation of MB} \quad (7)$$

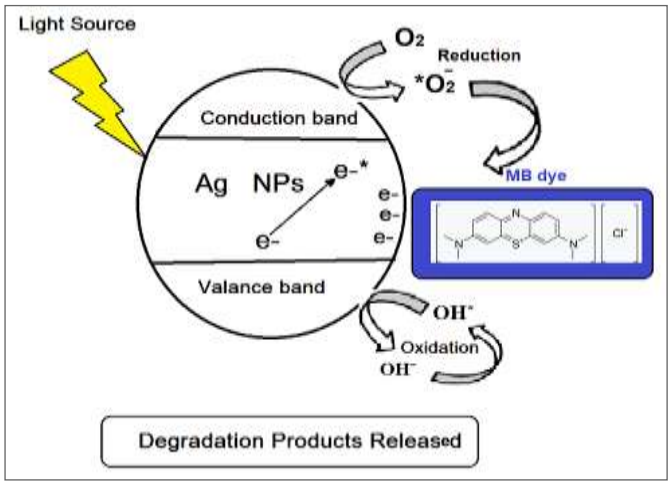

Figure 17. Schematic illustration of the photocatalytic performance of Ag NPs during MB dye degradation.
Source: Elaborated by the authors.

Methylene blue, with a molecular weight of 319.85 g/mol and the chemical formula $C_{16}H_{18}ClN_3S$, was used in this study as a model dye. Its removal was achieved through the combined effects of light and the catalyst (**Eq. 3**). The reaction occurs between the positively charged methylene blue molecules and the negatively charged surface of the catalyst at a pH of 10. In a basic medium with excess hydroxide ions (OH^-), photo-oxidation of hydroxyl radicals $^{\bullet}OH$ is facilitated by hole-pair formation on the catalyst surface as described by the reaction $h^+_{VB} + OH^- \rightarrow {}^{\bullet}OH$ (Li *et al.*, 2014). First, dissolved oxygen in the solution is converted into superoxide radicals ($O_2^{\bullet-}$) due to interactions with the photo-generated electrons (**Eq. 4**, **5**). Second, the dye interacts with the photogenerated holes, undergoes photo-oxidation, and is subsequently degraded and eventually mineralized (**Eq. 6**, **7**) (Altaf *et al.*, 2021; Khattar *et al.*, 2018). The degradation rate is high, which is attributed to the high purity and small size of the silver nanoparticles Ag NPs used in this study. The photodegradation efficiency (PDE) of Ag nanoparticles prepared in the presence of PVA stabilizer is recorded at 95.60%, which is close to the efficiency of the commercial standard silver (Fluka), which amounted to PDE 98.60%. This result highlights the effective role of PVA in improving the photocatalytic performance of the process.

4. Conclusions

Silver nanoparticles (NPs) have been successfully synthesized using an electrochemical method that is inexpensive, simple, and provides high precision in controlling the orientation, morphology and size, and dimensions at the nanometer scale. To enhance the catalytic performance in photolysis, silver nanoparticles prepared underwent calcination at 300 °C to promote crystallization growth. For the catalytic activity test, the silver nanoparticles prepared in the presence of the stabilizer PVA were selected due to their large surface area, and a small nanoparticle size of about 60.51 nm for use as a catalyst in photodegradation. The prepared silver NPs were compared with standard silver NPs (Fluka, Switzerland). The activation energy (Ea) values were determined as showing 14.737 kJ/mol for the standard silver NPs, and 13.483 kJ/mol for the prepared NPs. The photodegradation data of methylene blue (MB) solutions under thermodynamic analysis indicated that the positive $\Delta H^{o\#}$ confirmed an endothermic response, while the positive $\Delta G^{o\#}$ suggested a non-spontaneous process. Additionally, the negative $\Delta S^{o\#}$ indicates a decrease in entropy during activation. The interaction of reactive species, such as hydroxyl radicals ($^{\bullet}OH$) and superoxide ($O_2^{\bullet-}$), was generated during the photocatalytic process. The final degradation products of the dye breakdown catalyzed by the silver NPs were carbon dioxide (CO_2) and water (H_2O).

Authors' contribution

Conceptualization: Hayder Khudhair Khattar; **Data curation**: Hayder Khudhair Khattar; Zainab Abdel-Zahra Abdel-Hassan; **Formal Analysis**: Hayder Khudhair Khattar; **Funding acquisition**: Not applicable; **Investigation**: Hayder Khudhair Khattar; Zainab Abdel-Zahra Abdel-Hassan; **Methodology** Zainab Abdel-Zahra Abdel-Hassan; **Project administration**: Zainab Abdel-Zahra Abdel-Hassan; **Resources**: Hayder Khudhair Khattar; Zainab Abdel-Zahra Abdel-Hassan; **Software**: Zainab Abdel-Zahra Abdel-Hassan; **Supervision**: Emad Abbas Jaffar Al-Mulla; **Validation**: Emad Abbas Jaffar Al-Mulla; **Visualization**: Emad Abbas Jaffar Al-Mulla; **Writing – original draft**: Zainab Abdel-Zahra Abdel-Hassan; **Writing – review & editing**: Emad Abbas Jaffar Al-Mulla.

Conflict of interest

The authors declare and signs there is no conflict of interest involving this work.

Data availability statement

The data will be available upon request.

Artificial Intelligence usage statement

The authors declare that they did not use Artificial Intelligence tools at any stage of the preparation, correction, or evaluation of this work.

Funding

Not applicable.

Acknowledgments

Not applicable.

References

Abdellatif, A. A. H.; Alhathloul, S. S.; Aljohani, A. S. M.; Maswadeh, H.; Abdallah, E. M.; Musa, K. H.; El Hamd, M. A. Green Synthesis of Silver Nanoparticles Incorporated Aromatherapies Utilized For Their Antioxidant And Antimicrobial Activities Against Some Clinical Bacterial Isolates. *Bioinorganic Chemistry And Applications.* **2022**, *2022*, 432758. https://doi.org/10.1155/2022/2432758

Ahmad, I.; Aqil, F. (ed.). *New strategies combating bacterial infection*. John Wiley & Sons, 2008. https://doi.org/10.1002/9783527622931

Altaf, N. U. H.; Naza, M. Y.; Shukrullaha, S.; Bhattiet, H. N. Testing of photocatalytic potential of silver nanoparticles produced through nonthermal plasma reduction reaction and stabilized with saccharides. *Main Group Chemistry.* **2021**, *20* (4), 475-488. https://doi.org/10.3233/MGC-210059

Annamalai, J.; Nallamuthu, T. Green synthesis of silver nanoparticles: characterization and determination of antibacterial potency. *Applied nanoscience.* **2016**, *6*, 259-265. https://doi.org/10.1007/s13204-015-0426-6

Bharadwaj, K. K.; Rabha, B.; Pati, S.; Choudhury, B. K.; Sarkar, T.; Gogoi, S. K.; Kakati, N.; Baishya, D.; Kari, Z. A.; Edinur, H. A. Green Synthesis of Silver Nanoparticles Using Diospyros Malabarica Fruit Extract And Assessments of Their Antimicrobial, Anticancer and Catalytic Reduction Of 4-Nitrophenol (4-Np). *Nanomaterials.* **2021**, *11* (8), 1999. https://doi.org/10.3390/nano11081999

Bosoy, D.; Axelband, J.; Pursell, R. N.; Lukaszczyk, J J.; Stawicki, S. P. Utilization of methylene blue in the setting of hypotension associated with concurrent renal and hepatic failure: a concise review. *Opus.* **2008**, *12*, 21-29. https://doi.org/10.4103/IJAM.IJAM_88_16

Buendía-Otero, M. J.; Jiménez-Corzo, D. J.; Caamaño De Ávila, Z. I.; Restrepo, J. B. ChromatThis reference was not cited in the text.ographic analysis of phytochemicals in the peel of Musa paradisiaca to synthesize silver nanoparticles. *Revista Facultad de Ingeniería Universidad de Antioquia.* **2022**, *103*, 130-137. https://doi.org/10.17533/udea.redin.20210427

Chaluvaraju, K. C.; Prasad, A.; Sharon Esther, S.; Gagana, S. A Brief Review on Recrystallization of Clinically Important Drugs. *International Journal of Pharmaceutical Research*. **2022**, 14 (1), 09752366.

Fairuzi, A. A.; Bonnia, N. N.; Akhir, R. M.; Abrani, M. A.; Akil, H. M. Degradation of methylene blue using silver nanoparticles synthesized from imperata cylindrica aqueous extract. In: IOP conference series: earth and environmental science. *IOP Publishing.* **2018**, 012018. https://doi.org/10.1088/1755-1315/105/1/012018

Gadelmawla, E. S.; Koura, M. M.; Maksoud, T. M. A.; Elewa, I. M.; Soliman, H. H. Roughness parameters. *Journal of materials processing*

Technology. **2002**, *123* (1), 133-145. https://doi.org/10.1016/S0924-0136(02)00060-2

Ghobashy, M. M.; Elkodous, M. A.; Shabaka, S. H.; Sherif, A. Y.; Alshangiti, D. M.; Madani, M.; Al-Gahtany, S. A.; Walid F. Elkhatib, W. F.; Noreddin, A. M.; Nady, N.; El-Sayyad, G. S. An Overview of Methods for Production And Detection Of Silver Nanoparticles, With Emphasis On Their Fate And Toxicological Effects On Human, Soil, And Aquatic Environment. *Nanotechnology Reviews.* **2021**, *10* (1), 954-977. https://doi.org/10.1515/ntrev-2021-0066

Haryono, A.; Sondari D.; Harnami, S. B.; Randy, M. Sistesa Nanopartikel Perak Dan Potensi Aplikasinya. *Indonesian Journal of Industrial Research.* **2008**, *2* (3), 156-163.

Ho, J.-Y.; Huang, M. H. Synthesis of submicrometer-sized Cu_2O crystals with morphological evolution from cubic to hexapod structures and their comparative photocatalytic activity. *The Journal of Physical Chemistry C.* **2009**, *113* (32), 14159-14164. https://doi.org/10.1021/jp903928p

Jyoti, K.; Singh, A. Green synthesis of nanostructured silver particles and their catalytic application in dye degradation. *Journal of Genetic Engineering and Biotechnology.* **2016**, *14* (2), 311-317. https://doi.org/10.1016/j.jgeb.2016.09.005

Khattar, H. K.; Juda, A. M.; Al-Saady, F. A. A. Preparation of Cu_2O nanoparticles as a catalyst in photocatalyst activity using a simple electrodeposition route. *Nano Biomed. Eng.* **2018**, *10* (4), 406-416. https://doi.org/10.5101/nbe.v10i4.p406-416

Khedkar, C. V.; Vedpathak, A. S.; Dhotre, A. V.; Daware, K. D.; Kolekar, Y. D.; Sartale, S. D.; Gosavi, S. W.; Patil, S. I. Synthesis, Characterization, Electrochemical and Catalytic Performance Of Nio Nanostructures And Ag-Nio Nanocomposite. *Chemical Physics Impact.* **2023**, *6,* 100153. https://doi.org/10.1016/j.chphi.2022.100153

Kulkarni, A. A.; Bhanage, B. M. Ag@AgCl nanomaterial synthesis using sugar cane juice and its application in degradation of Azo dyes. *ACS Sustainable Chem. Eng.* **2014**, *2*, 1007-1013. https://doi.org/10.1021/sc4005668

Kuo, C.-H.; Huang, M. H. Facile synthesis of Cu_2O nanocrystals with systematic shape evolution from cubic to octahedral structures. *The Journal of Physical Chemistry C.* **2008**, *112* (47), 18355-18360. https://doi.org/10.1021/jp8060027

Li, Y.; Wu, W.; Dai, P.; Zhang, L.; Sun, Z.; Li, G.; Wu, M.; Chen, X.; Chen; C. WO_3 and Ag nanoparticle co-sensitized TiO_2 nanowires: preparation and the enhancement of photocatalytic activity. *RSC advances.* **2014**, *4* (45), 23831-23837. https://doi.org/10.1039/C4RA02161D

Lyu, L.-M.; Wang, W.-C.; Huang, M. H. Synthesis of Ag_2O nanocrystals with systematic shape evolution from cubic to hexapod structures and their surface properties. *Chemistry–A European Journal.* **2010**, *16* (47), 14167-14174. https://doi.org/10.1002/chem.201000563

Meena, J.; Santhakumar, K. An overview of a sustainable approach to the biosynthesis of AgNPs for electrochemical sensors. *Arabian Journal of Chemistry*. **2022**, 104324. https://doi.org/10.1016/j.arabjc.2022.104324

Mirsalari, S. A.; Nezamzadeh-Ejhieh, A. The catalytic activity of the coupled CdS-AgBr nanoparticles: a brief study on characterization and its photo-decolorization activity towards methylene blue. *Desalination Water Treat.* **2020**, *175*, 263-272. https://doi.org/10.5004/dwt.2020.24902

Munesh, S.; M, R. C. Photocatalytic decolorization of Acid Red 186 using alternative developed photocatalyst MBIR Dowex 11. *Research Journal of Chemical Sciences*. **2012**, *2* (9), 56-62.

Naganthran, A.; Verasoundarapandian, G.; Khalid, F. E.; Zulkharnain, A.; Nawawi, N. M.; Karim, M.; Mas Jaffri Masarudin, M. J.; Abdullah, C. A. C.; Ahmad, S. A. Synthesis, Characterization and Biomedical Application of Silver Nanoparticles. *Materials.* **2022**, *15* (2), 427. https://doi.org/10.3390/ma15020427

Nia, P. M.; Meng, W. P.; Alias, Y. Hydrogen peroxide sensor: Uniformly decorated silver nanoparticles on polypyrrole for wide detection range. *Applied Surface Science.* **2015**, *357*, 1565-1572. https://doi.org/10.1016/j.apsusc.2015.10.026

Ponsanti, K.; Tangnorawich, B.; Ngernyuang, N.; Pechyen, C. A flower shape-green synthesis and characterization of silver nanoparticles (AgNPs) with different starch as a reducing agent. *Journal of Materials Research and Technology.* **2020**, *9* (5), 11003-11012. https://doi.org/10.1016/j.jmrt.2020.07.077

Rabiei, M. Comparing methods for calculating nano crystal size of natural hydroxyapatite using X-ray diffraction. *Nanomaterials.* **2020**, *10* (9), 1627. https://doi.org/10.3390/nano10091627

Raposo, M.; Ferreira, Q.; Ribeiro, P. A. A guide for atomic force microscopy analysis of soft-condensed matter. *Modern research and educational topics in microscopy*. **2007**, *1*, 758-769.

Roco, M. C.; Mirkin, C. A.; Hersam, M. C. Nanotechnology research directions for societal needs in 2020: summary of international study. *Journal of nanoparticle research.* **2011**, *13*. 897-919. https://doi.org/10.1007/s11051-011-0275-5

Rodriguez-Sanchez, L.; Blanco, M. C.; López-Quintela, M. A. Electrochemical synthesis of silver nanoparticles. *The Journal of Physical Chemistry B.* **2000**, *104* (41), 9683-9688. https://doi.org/10.1021/jp001761r

Saeed, K.; Khan, I.; Shah, T.; Park, S.-Y. Synthesis, characterization and photocatalytic activity of silver nanoparticles/amidoxime-modified polyacrylonitrile nanofibers. *Fibers and Polymers.* **2015**, *16*, 1870-1875. https://doi.org/10.1007/s12221-015-5373-z

Sati, A.; Ranade, T. N.; Mali, S. N.; Ahmad Yasin, H. K.; Pratap, A. Silver nanoparticles (AgNPs): comprehensive insights into bio/synthesis, key influencing factors, multifaceted applications, and toxicity─ a 2024 update. *ACS omega.* **2025**, *10* (8), 7549-7582. https://doi.org/10.1021/acsomega.4c11045

Shanks, G. D. Control and elimination of Plasmodium vivax. *Advances in parasitology.* **2012**, *80*, 301-341. https://doi.org/10.1016/B978-0-12-397900-1.00006-2

Shende, S.; Gade, A.; Rai, M. Large-scale synthesis and antibacterial activity of fungal-derived silver nanoparticles. *Environmental Chemistry Letters.* **2017**, *15*, 427-434. https://doi.org/10.1007/s10311-016-0599-6

Shuaib, U.; Hussain, T.; Ahmad, R.; Zakaullah, M.; Mubarik, F. E.; Tul Muntaha, S.; Ashrafet, S. Plasma-liquid synthesis of silver nanoparticles and their antibacterial and antifungal applications. *Materials Research Express.* **2020**, *7* (3), 035015. https://doi.org/10.1088/2053-1591/ab7cb6

Sinha, T. R.; Ahmaruzzaman, M.; Bhattacharjee, A. A green and facile synthesis of silver nanoparticles and its application in the reduction and photodegradation of organic compounds. *Indian J. Chem. Technol.* **2016**, *23*, 462-468.

Stewart, B. W. K. P.; Christopher, P. W. *International agency for research on cancer*. World cancer report 2014, 2014.

Tkach, V. V.; Kushnir, M.; de Oliveira, S.; Verbovetska, A.; Kusyak, N.; Kusyak, A.; Dytynchenko, I.; Olímpio, A.; Yagodynets´, P. The theoretical description for methylene blue electrochemical determination and decolorization, assisted by polynaphthoquinones/Ti/TiO_2/VO (OH) composite. *Applied Journal of Environmental Engineering Science.* **2020**, *6* (1), 14-21.

Wang, W.; Xiao, K.; He, T.; Zhu, L. Synthesis and characterization of Ag nanoparticles decorated mesoporous sintered activated carbon with antibacterial and adsorptive properties. *J. Alloys Compd.* **2015**, *647*, 1007-1012. https://doi.org/10.1016/j.jallcom.2015.05.180

WHO (World Health Organization). *World Health Organization model list of essential medicines*: 21st list 2019. World Health Organization, 2019.

Xue, C.-H.; Jia, C.; Wei, Y.; Shuntian, J.; Jianzhong, M. Superhydrophobic conductive textiles with antibacterial property by coating fibers with silver nanoparticles. *Applied surface science.* **2012**, *258* (7), 2468-2472. http://dx.doi.org/10.1016/j.apsusc.2011.10.074

Yin, B.; Ma, H.; Wang, S.; Chen, S. Electrochemical synthesis of silver nanoparticles under protection of poly (N-vinylpyrrolidone). *The Journal of Physical Chemistry B.* **2003**, *107* (34), 8898-8904. https://doi.org/10.1021/jp0349031

Yin, D.; Liu, Y., Chen, P.; Meng, G.; Huang, G.; Cai, L.; Zhang, L. Controllable synthesis of silver nanoparticles by the pulsed electrochemical deposition in a forced circulation reactor. *International Journal of Electrochemical Science.* **2020**, *15* (4), 3469-3478. https://doi.org/10.20964/2020.04.57

Zhang, X.-F.; Liu, Z-G.; Shen, W.; Gurunathan, S. Silver nanoparticles: synthesis, characterization, properties, applications, and therapeutic approaches. *International journal of molecular sciences.* **2016**, *17* (9), 1534. https://doi.org/10.3390/ijms17091534

Zhang, Z.; Zhao, B.; Hu, L. PVP protective mechanism of ultrafine silver powder synthesized by chemical reduction processes. *Journal of Solid State Chemistry.* **1996**, *121* (1), 105-110. https://doi.org/10.1006/jssc.1996.0015